

A Stochastic Nonlinear Water Wave Model for Efficient Uncertainty Quantification

Daniele Bigoni · Allan P. Engsig-Karup ·
Claes Eskilsson

Received: date / Accepted: date

Abstract A major challenge in next-generation industrial applications is to improve numerical analysis by quantifying uncertainties in predictions. In this work we present a stochastic formulation of a fully nonlinear and dispersive potential flow water wave model for the probabilistic description of the evolution waves. This model is discretized using the Stochastic Collocation Method (SCM), which provides an approximate surrogate of the model. This can be used to accurately and efficiently estimate the probability distribution of the unknown time dependent stochastic solution after the forward propagation of uncertainties. We revisit experimental benchmarks often used for validation of deterministic water wave models. We do this using a fully nonlinear and dispersive model and show how uncertainty in the model input can influence the model output. Based on numerical experiments and assumed uncertainties in boundary data, our analysis reveals that some of the known discrepancies from deterministic simulation in comparison with experimental measurements could be partially explained by the variability in the model input. This type of stochastic analysis is relevant for computationally intensive problems where traditional methods, such as Monte Carlo type methods, are intractable due to their slow convergence. The Stochastic Collocation Method exhibits faster convergence and retains the non-intrusive properties of Monte Carlo methods, allowing for the straight forward use of massively parallel computing.

Keywords Uncertainty Quantification · generalized Polynomial Chaos · heterogeneous computing · high-performance computing · free surface water waves · Laplace problem · partial differential equations.

D. Bigoni · A.P. Engsig-Karup
Department of Applied Mathematics and Computer Science, Technical University of Denmark, 2800 Kgs. Lyngby, Denmark
E-mail: dabi@dtu.dk

C. Eskilsson
Department of Shipping and Marine Technology, Chalmers University of Technology, SE-412 96 Gothenburg, Sweden

1 Introduction

In coastal and offshore engineering it is important to design maritime structures that can withstand critical failures due to wave-induced loadings. The most extreme wave induced-loadings can be estimated from direct measurements, laboratory experiments and simulation-based tools which can account for the wave kinematics sufficiently accurately. It is still common to predict wave kinematics using numerical tools which have been validated by single or few deterministic simulations and compared to idealized physical experiments, e.g., in wave tanks. In an era with fast growing computing power, computational simulation tools are increasingly being used for engineering studies and analysis. In particular, this trend is driven by improvements in hardware which have seen a recent paradigm shift from single to many core computations. Parallel to this shift, there is an increased focus on making simulation tools more reliable by estimation and reduction of uncertainty in results delivered by such tools. This requires a shift from deterministic approaches to probabilistic approaches [35]. This is of immense importance for tools that are used for critical decision support, risk management and risk analysis.

The research field of Uncertainty Quantification deals with mathematical techniques that can improve engineering analysis in model-based simulation tools. The goal is to deliver confidence intervals and estimation of probability distributions of Quantities of Interest (QoIs) to describe the likelihood for the QoIs to take a given value. The analysis of uncertainty in dynamical systems can be split in four steps:

- (a) Deterministic modeling and identification of Quantities of Interest (QoI) and sources of uncertainty
- (b) Quantification of uncertainty sources by means of probability distributions
- (c) Uncertainty propagation through the system
- (d) Sensitivity analysis

This work will deal with the first three of these steps, where classical benchmarks, such as [1,10], will be used as deterministic models and different QoI will be investigated for the different problems (step a). In coastal and offshore engineering, the QoIs are typically local wave statistics for average or maximum heights, loads, etc. The analysis of such QoIs is useful for risk management aimed at reducing risk in design and operations. For example, in structural engineering Ultimate Limits State (ULS) design are today based on load and resistance factors determined using statistics obtained based on measured data or experiments.

Due to the lack of data, some assumptions will be made about the probability distributions of the sources of uncertainty (step b), that in hydrodynamics simulations are commonly inlet/outlet conditions (boundary conditions), bathymetry data and structural positions (geometry). All these uncertainties can be classified as *epistemic* [19], because they can in principle be reduced either by better measurements and/or, in case of experimental tests, by more accurate settings. The step (c) will be the main focus of this work, where the

propagation of the probability distributions through the dynamical system will be investigated. Traditional sampling techniques, such as Monte Carlo methods, will be compared to modern techniques based on generalized Polynomial Chaos [36]. Non-intrusive approaches such as Stochastic Collocation and Sparse Grids will be preferred to intrusive approaches, due to the ability of the former of re-using existing code, avoiding the need for re-engineering existing software. The step (d) concerns with the identification of the sources of uncertainty that give the biggest contribution to the uncertainty of the QoI. This topic will not be covered here, but its application is based on all the techniques used in (c).

Uncertainty quantification in coastal and offshore engineering is challenged by the requirements of computational resources for single deterministic simulations. Recent works [27] have explored the usage of Monte Carlo type methods for the estimation of extreme responses. However, these methods show a very slow convergence rate and even with the disruptive introduction of many-core hardware and parallel simulation tools [13,12,17], they become quickly intractable, because few simulations are affordable in general. Thus, techniques with fast convergence, such as the Stochastic Collocation Method become very important in this setting as well as in many other engineering areas dominated by heavy computational requirements.

1.1 Paper contributions

We propose a stochastic formulation of a fully nonlinear and dispersive potential flow model for efficient uncertainty quantification. We revisit classical benchmarks and propose to use the stochastic collocation method for ensuring that the ensemble of solutions can be generated independently using standard deterministic solvers as black-box methods with tunable parameters. The outcome is a set of stochastic benchmarks. The analysis reveals opportunities and challenges in practical uncertainty quantification that needs to be addressed for computationally intensive computer simulation and engineering analysis.

1.2 Paper organization

The paper will be organized as follows. In Section 2 we introduce the governing equation for the deterministic description of nonlinear water waves based on potential theory. In Section 3 we describe how a stochastic model can be formulated, including a description of the Stochastic Collocation Method (SCM) approach for creating approximate generalized Polynomial Chaos (gPC) surrogate models of the solutions. In Section 4, the effect of parametric uncertainty in bathymetry and wave input are studied and numerical experiments are compared for traditional sampling and SCM approaches.

2 Mathematical formulation

We consider unsteady water waves described by a potential model for three-dimensional fully nonlinear and dispersive free surface flows under the influence of gravity. The flow is assumed inviscid and irrotational. It can, without simplifications, be used for short and long wave propagation in both shallow and deep water where viscous and rotational effects are negligible. The sea bed is assumed variable and impermeable.

We introduce a Cartesian coordinate system (x, y, z) with (x, y) the horizontal and z the vertical dimensions, where the z coordinate points upwards. The functions $h(x, y)$ and $\zeta(t, x, y)$ describe respectively the depth of the sea bed and the free surface. The still water level is given by $z = 0$.

2.1 The deterministic model

The evolution of water waves over an arbitrary sea bed are described by the kinematic and dynamic free surface boundary conditions¹

$$\partial_t \zeta(\mathbf{x}, t) = -\nabla \zeta \cdot \nabla \tilde{\phi} + \tilde{w}(1 + \nabla \zeta \cdot \nabla \zeta), \quad (1a)$$

$$\partial_t \tilde{\phi}(\mathbf{x}, t) = -g\zeta - \frac{1}{2} \left(\nabla \tilde{\phi} \cdot \nabla \tilde{\phi} - \tilde{w}^2(1 + \nabla \zeta \cdot \nabla \zeta) \right), \quad (1b)$$

where $\nabla = (\partial_x, \partial_y)$. We will consider waves in a spatial domain $D \in \mathbb{R}^l$ (fluid volume), $l = 2, 3$ and a time domain $t \in [0, T]$ with final time $T > 0$. For the fluid volume, a Laplace problem defines the scalar velocity potential

$$\phi = \tilde{\phi}, \quad z = \zeta(\mathbf{x}, t), \quad (2a)$$

$$\nabla^2 \phi + \partial_{zz} \phi = 0, \quad -h \leq z < \zeta(\mathbf{x}, t), \quad (2b)$$

$$\partial_z \phi + \nabla h \cdot \nabla \phi = 0, \quad z = -h. \quad (2c)$$

Using a classical σ -transformation

$$\sigma \equiv \frac{z + h(\mathbf{x})}{d(\mathbf{x}, t)}, \quad 0 \leq \sigma \leq 1, \quad (3)$$

the Laplace problem can be written as

$$\Phi = \tilde{\phi}, \quad \sigma = 1, \quad (4a)$$

$$\nabla^2 \Phi + \nabla^2 \sigma (\partial_\sigma \Phi) + 2\nabla \sigma \cdot \nabla (\partial_\sigma \Phi) + (\nabla \sigma \cdot \nabla \sigma + (\partial_z \sigma)^2) \partial_{\sigma\sigma} \Phi = 0, \quad 0 \leq \sigma < 1, \quad (4b)$$

$$\mathbf{n} \cdot (\nabla, \partial_z \sigma \partial_\sigma) \Phi = 0, \quad (\mathbf{x}, \sigma) \in \partial\Omega, \quad (4c)$$

¹ The gravitational acceleration constant, g , is set to be 9.81 m/s^2 .

where

$$\nabla\sigma = \frac{1-\sigma}{d}\nabla h - \frac{\sigma}{d}\nabla\zeta, \quad (5a)$$

$$\nabla^2\sigma = \frac{1-\sigma}{d}(\nabla^2 h - \frac{\nabla h \cdot \nabla h}{d}) - \frac{\sigma}{d}(\nabla^2\zeta - \frac{\nabla\zeta \cdot \nabla\zeta}{d}) - \frac{1-2\sigma}{d^2}\nabla h \cdot \nabla\zeta - \frac{\nabla\sigma}{d} \cdot (\nabla h + \nabla\zeta), \quad (5b)$$

$$\partial_z\sigma = \frac{1}{d}. \quad (5c)$$

The relation between the scalar velocity potential function and velocity field is

$$(\mathbf{u}, w) = (\nabla + \nabla\sigma\partial_\sigma, \partial_z\sigma\partial_\sigma)\Phi. \quad (6)$$

The governing equations can be solved in the setting of a numerical wave tank and is then subject to initial and boundary conditions

$$\zeta(\mathbf{x}, t=0) = \phi(\mathbf{x}, t=0) = 0, \quad \partial_n\zeta = \partial_n\phi = 0, \quad x \in \partial D \setminus \bar{D}^{FS}, \quad (7)$$

where wave generation and absorption is done using a line relaxation method [21]. A complete derivation of the equations are given in [12]. These model equations can be solved numerically using flexible-order finite differences [11, 13] and the massively parallel implementation [17] enables fast hydrodynamics computations [12]. A fast solver is a prerequisite for enabling stochastic analysis with acceptable time frames and can be used to deliver improved engineering analysis in maritime applications.

2.2 The stochastic model

Following [36], a stochastic formulation is obtained by introducing $\omega \in \Omega$ as random input of the system defined in the probability space $(\Omega, \mathcal{F}, \mathcal{P})$, where Ω is the sample space, \mathcal{F} is a σ -field and \mathcal{P} is a probability measure. This makes the unknown solution a random process $\zeta(\mathbf{x}, t, \omega) : \bar{D}^{FS} \times [0, T] \times \Omega \rightarrow \mathbb{R}$ and $\phi(\mathbf{x}, t, \omega) : \bar{D} \times [0, T] \times \Omega \rightarrow \mathbb{R}$. \bar{D} is the closed spatial domain volume with FS indicating the restriction to the free surface, $\bar{D} = \{\mathbf{x} | \mathbf{x} \in \xi\}$.

A parametrization of the stochastic model is required in order to solve it numerically. A set of random variables $\mathbf{Z} : \Omega \rightarrow \mathbb{R}^d$, is introduced to characterize random inputs, where $d \geq 1$ is the stochastic dimension.

The stochastic reformulation of the deterministic system (1) is

$$\partial_t\zeta(\mathbf{x}, t, \mathbf{Z}) = -\nabla\zeta \cdot \nabla\tilde{\phi} + \tilde{w}(1 + \nabla\zeta \cdot \nabla\zeta), \quad (8a)$$

$$\partial_t\tilde{\phi}(\mathbf{x}, t, \mathbf{Z}) = -g\zeta - \frac{1}{2}(\nabla\tilde{\phi} \cdot \nabla\tilde{\phi} - \tilde{w}^2(1 + \nabla\zeta \cdot \nabla\zeta)), \quad (8b)$$

where for any realization of an uncertain sea state, the Laplace problem (2) is fulfilled to obtain closure.

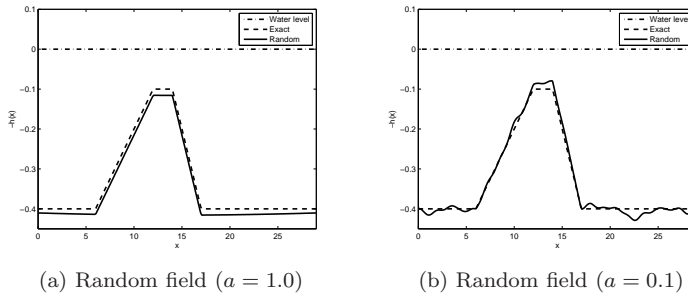


Fig. 1: Possible topographies of the bottom floor in the submerged bar experiment. Figures 1a and 1b show two realizations of the KL-expanded random fields (9) with different correlation lengths $a = 1$ and $a = 0.1$ respectively, where the total variance represented is ≥ 0.95 .

2.3 Dimensionality reduction using the Karhunen-Loève Expansion

As an example, in the wave model, the bathymetry function describing still-water depth can be uncertain and therefore be treated as a random field. The Karhunen-Loève expansion (KLE) is a useful technique for dimension reduction that can be used for the parametrization of such random fields [22, 30]. Let $h(\mathbf{x}, \omega)$ be a spatially varying random field over a spatial domain Ω with mean $\mu_h(\mathbf{x})$ and covariance function $C(\mathbf{x}_1, \mathbf{x}_2) = \mathbf{Cov}(h(\mathbf{x}_1, \omega), h(\mathbf{x}_2, \omega))$. Then the bathymetry function $h(\mathbf{x}, \omega)$ can be parametrized as an infinite series

$$h(\mathbf{x}, \omega) = \mu_h(\mathbf{x}) + \sum_{i=1}^{\infty} \sqrt{\lambda_i} \psi_i(\mathbf{x}) Y_i(\omega), \quad (9)$$

where $\mathbf{E}[Y_i(\omega)] = 0$, $\mathbf{Cov}[Y_i, Y_j] = \delta_{ij}$ and $\{\lambda_i, \psi_i\}_{i=1}^{\infty}$ are the solutions of the generalized eigenvalue problem

$$\int_{\Omega} C(\mathbf{x}, \mathbf{s}) \psi_i(\mathbf{s}) d\mathbf{s} = \lambda_i \psi_i(\mathbf{x}). \quad (10)$$

If $h(\mathbf{x}, \omega)$ is a Gaussian random field, then $Y_i \sim \mathcal{N}(0, 1)$.

For practical computations (9) is truncated at a desired order N . It is easy to check how much of the variance of the original random field is retained by such approximation, using that

$$\begin{aligned} \mathbf{Var}[h_N(\mathbf{x}, \omega)] &= \mathbf{E}[h_N^2(\mathbf{x}, \omega)] - \mathbf{E}[h_N(\mathbf{x}, \omega)]^2 \\ &= \mathbf{E}\left[\sum_{i,j=1}^N \sqrt{\lambda_i \lambda_j} \psi_i(\mathbf{x}) \psi_j(\mathbf{x}) Y_i(\omega) Y_j(\omega)\right] = \sum_{i=1}^N \lambda_i \psi_i^2(\mathbf{x}), \end{aligned}$$

where the orthogonality of $\{Y_i\}_{i=1}^N$ is exploited. There are several options regarding the correlation kernel $C(\mathbf{x}_1, \mathbf{x}_2)$. All these are problem dependent and

an appropriate characterization of the random field has to be performed prior to the construction of the KL-expansion. In this work, we will use the exponential covariance kernel

$$C(\mathbf{x}_1, \mathbf{x}_2) = \exp\left(-\frac{\|\mathbf{x}_1 - \mathbf{x}_2\|}{a}\right), \quad (11)$$

where a is the correlation length. Figure 1 shows realizations of the KL-expansions of a 1D random field $h(x, \omega)$ for the submerged bar experiment considered in section 4.1 with exponential covariance kernel and zero mean for different correlation length a . The total variance represented by the KL-expansions $h_N(x, \omega)$ is fixed to 0.95 (the total variance of $h(x, \omega)$ with exponential covariance kernel is 1). In Figure 1a and 1b, fields with different correlation lengths are illustrated. Shorter correlation lengths determine a slower decay of the expansion coefficients in (9) and thus a longer expansion is required to express higher local variability.

3 Uncertainty Quantification

In Uncertainty Quantification we are interested in studying the propagation of uncertainties through the stochastic dynamical system (8). To reduce the notation used, let $\mathbf{u}(\mathbf{x}, t, \mathbf{Z}) = [\zeta(\mathbf{x}, t, \mathbf{Z}), \tilde{\phi}(\mathbf{x}, t, \mathbf{Z})]^T$. We are interested in describing the stochastic result in terms of its probability distribution and/or its first moments, e.g., mean and variance

$$\mathbf{E}[\mathbf{u}(\mathbf{x}, t, \mathbf{z})] = \int_{\mathbb{R}^d} \mathbf{u}(\mathbf{x}, t, \mathbf{z}) dF_{\mathbf{z}}(\mathbf{z}) = \int_{\mathbb{R}^d} \mathbf{u}(\mathbf{x}, t, \mathbf{z}) \rho_{\mathbf{z}}(\mathbf{z}) d\mathbf{z} = \mu_{\mathbf{u}}(\mathbf{x}, t), \quad (12)$$

$$\mathbf{Var}[\mathbf{u}(\mathbf{x}, t, \mathbf{z})] = \int_{\mathbb{R}^d} (\mathbf{u}(\mathbf{x}, t, \mathbf{z}) - \mu_{\mathbf{u}}(\mathbf{x}, t))^2 \rho_{\mathbf{z}}(\mathbf{z}) d\mathbf{z}, \quad (13)$$

where $\rho_{\mathbf{z}}(\mathbf{z})$ and $F_{\mathbf{z}}(\mathbf{z})$ are the Probability Density Function (PDF) and the Cumulative Distribution Function (CDF) of the random vector \mathbf{Z} .

In this work we will focus exclusively on non-intrusive methods, which require a minimal development effort. In particular the existing solvers are considered as black boxes and the non-intrusive methods need only to be wrapped around them. On the contrary, intrusive methods require the development of new solvers based on mixed discretization of the stochastic and the spatial models. These methods are usually better in dynamically adapting to time-dependent problems [7, 6, 4, 32, 29] but their implementation is often very demanding – sometimes prohibitive – for existing customized non-linear solvers.

3.1 Pseudo-random sampling methods

Among the existent techniques for Uncertainty Quantification, the random sampling methods are the most widely used. The most notable of these techniques, is the Monte Carlo method, developed in the late 40s. It is based

on the law of large numbers and it states that given the random vector $\mathbf{u} : \bar{D} \times (0, T] \times \mathbb{R}^d \rightarrow \mathbb{R}^m$ and the functional $g : \mathbb{R}^m \rightarrow \mathbb{R}^m$,

$$\frac{1}{n} \sum_{i=1}^n g(\mathbf{u}(\mathbf{x}, t, \mathbf{z}^{(i)})) \xrightarrow{a.s.} \mathbf{E}[g(\mathbf{u}(\mathbf{x}, t, \mathbf{Z}))] = \int_{\mathbb{R}^d} g(\mathbf{u}(\mathbf{x}, t, \mathbf{z})) dF_{\mathbf{z}}(\mathbf{z}), \quad (14)$$

for $n \rightarrow \infty$. In the definition above $\{\mathbf{z}^{(i)}\}_{i=1}^n$ is an ensemble of samples drawn from the probability distribution of \mathbf{Z} and a.s. stands for *almost surely* implying convergence in probability. The implication of this property is that the realizations are always assumed meaningful. For $g_1 : \mathbf{u} \mapsto \mathbf{u}$ and $g_2 : \mathbf{u} \mapsto (\mathbf{u} - \mu_{\mathbf{u}})^2$,

$$\mathbf{E}[\mathbf{u}(\mathbf{x}, t, \mathbf{Z})] = \mathbf{E}[g_1(\mathbf{u}(\mathbf{x}, t, \mathbf{Z}))] \approx \frac{1}{n} \sum_{i=1}^n g_1(\mathbf{u}(\mathbf{x}, t, \mathbf{z}^{(i)})) = \bar{\mu}_{\mathbf{u}}(\mathbf{x}, t), \quad (15)$$

$$\mathbf{Var}[\mathbf{u}(\mathbf{x}, t, \mathbf{Z})] = \mathbf{E}[g_2(\mathbf{u}(\mathbf{x}, t, \mathbf{Z}))] \approx \frac{1}{n} \sum_{i=1}^n g_2(\mathbf{u}(\mathbf{x}, t, \mathbf{z}^{(i)})) = \bar{\sigma}_{\mathbf{u}}^2(\mathbf{x}, t). \quad (16)$$

The probabilistic error of these approximations is reduced asymptotically as $\mathcal{O}(1/\sqrt{n})$ for number of realizations growing, i.e. $n \rightarrow \infty$. In spite of this slow convergence rate, Monte Carlo methods are widely used [27] due to their robustness, ease of use and to the fact that they do not suffer the *curse of dimensionality*, i.e., their convergence rate is independent from d . Due to all these properties, MC method is useful to generate reference solutions and for comparison with other techniques, but not for intractable problems that require significant effort. Thus, with the present technology, MC method cannot be used for all problems despite its robustness.

The slow convergence rate means that the ensemble size needed to resemble the target distribution must be large. Improvements of the Monte Carlo method have been proposed in order to cover more uniformly the stochastic domain, obtaining improved convergence rates, not always in the worst case scenarios, but in the average scenarios.

One of these methods is the Latin Hyper Cube method (LHC) [25], where the stochastic domain is divided in n equiprobable bins along each dimension and samples are taken such that each bin contains only one sample. This produces an ensemble that covers more uniformly the stochastic space and provides a better convergence rate in the average cases, even if the worst case convergence rate remains $\mathcal{O}(1/\sqrt{n})$. A drawback of LHC is that the sample size needs to be known a priori, and thus it is not suitable for incremental sampling.

An other notable method is the Quasi Monte Carlo (QMC) [26], where low discrepancy sequences of points are generated such that the domain is uniformly covered. The convergence rate of QMC is improved to $\mathcal{O}(\ln(n)^d/n)$, but the stochastic dimensionality of the problem becomes important.

3.2 Deterministic sampling methods

In the following we will handle functions with finite variance, i.e. belonging to the weighted $L^2_{\rho_{\mathbf{z}}}$ space defined as

$$L^2_{\rho_{\mathbf{z}}} = \left\{ f : \mathbb{R}^d \rightarrow \mathbb{R} \mid \int_{\mathbb{R}^d} f^2(\mathbf{z}) \rho_{\mathbf{z}} d\mathbf{z} = \mathbf{Var}[f(\mathbf{Z})] < \infty \right\}, \quad (17)$$

with inner product and norm defined as

$$(f, g)_{\rho_{\mathbf{z}}} = \int_{\mathbb{R}^d} f(\mathbf{z})g(\mathbf{z})\rho_{\mathbf{z}}d\mathbf{z}, \quad \|f\|_{\rho_{\mathbf{z}}} = \sqrt{(f, f)_{\rho_{\mathbf{z}}}}. \quad (18)$$

For many standard distributions with density $\rho_{\mathbf{z}}$, we can find $\{\Phi_i(\mathbf{z})\}_{i=0}^N \subset \mathbb{P}^N$ that form a basis for $L^2_{\rho_{\mathbf{z}}}$ [38, 37]. If the distribution is not standard, but has a density, then one can still use Gram-Schmidt orthogonalization to create suitable polynomials (see [16, 15]). We can then define a projection operator P_N from $L^2_{\rho_{\mathbf{z}}}$ onto $\text{span}\{\Phi_i(\mathbf{z})\}_{i=0}^N$ as

$$f(\mathbf{z}) \approx \tilde{f}(\mathbf{z}) = P_N f(\mathbf{z}) = \sum_{i=0}^N \hat{f}_i \Phi_i(\mathbf{z}), \quad \hat{f}_i = \frac{(f, \Phi_i)_{\rho_{\mathbf{z}}}}{\|\Phi_i\|_{\rho_{\mathbf{z}}}}. \quad (19)$$

This provides an approximation \tilde{f} of the target function f that is known as the *generalized Polynomial Chaos (gPC) expansion* of f . This gPC-expansion can be thought as a *surrogate function* of f . The computation of statistics from such surrogate function can be done easily. For example,

$$\mathbf{E}[f(\mathbf{z})] \approx \mathbf{E}[\tilde{f}(\mathbf{z})] = \hat{f}_0, \quad (20)$$

$$\mathbf{Var}[f(\mathbf{z})] \approx \mathbf{Var}[\tilde{f}(\mathbf{z})] = \sum_{i=1}^N \hat{f}_i^2 \|\Phi_i\|_{\rho_{\mathbf{z}}}^2, \quad (21)$$

where orthogonality of the basis $\{\Phi_i(\mathbf{z})\}_{i=0}^N$ is exploited.

The convergence of the polynomial approximation in (19) is spectral (super linear) if f is a smooth function and otherwise algebraic, cf. [16, 5]. In order to obtain the surrogate model in (19), we are left with the computation of the coefficients \hat{f}_i in (19). These can be obtained by means of two methods: the *Galerkin method*, where a reformulation of (8) in terms of stochastic modes is required, or the *Collocation method*, where approximations of \hat{f}_i 's are obtained by solving (8) on carefully selected points in the stochastic space. The Galerkin method is *intrusive*, i.e. the problem needs to be reformulated, thus it is cumbersome to be carried out for complex systems and will not be covered in this work (see [37, 24] for an introduction to stochastic Galerkin methods). On the contrary the collocation method is *non-intrusive* and thus any existing deterministic solver for (1) can be used without modification.

3.2.1 Stochastic Collocation Method

The idea of the stochastic collocation method is to produce an ensemble of solutions $\mathbf{u}^{(j)}$, $i = 1, \dots, M$ obtained by deterministically solving the governing equations (8) subject to carefully selected choices of M parameters $S_N = \{\mathbf{z}^{(j)}\}_{j=1}^M$ in the stochastic domain, in order to enable high accuracy in the evaluation of the coefficients of the gPC-expansion (19). An alternative approach is the interpolation method, but this is out of the scope of this work (see [37, 24]). In order to simplify the notation in the following, we start considering functions of one stochastic parameter in the $L^2_{\rho_z}$ space (17), i.e. $d = 1$.

A set of orthogonal polynomials $\{\phi_i(z)\}_{i=0}^N$ that form a basis for $L^2_{\rho_z}$ can be found as explained in the preceding section. The expansion coefficients in (19) can then be found approximately as

$$\hat{u}_i = \frac{(u, \phi_i)_{\rho_z}}{\|\phi_i\|_{\rho_z}} = \frac{\int_{\mathbb{R}} u(z) \phi_i(z) \rho_z(z) dz}{\int_{\mathbb{R}} \phi_i^2(z) \rho_z(z) dz} \approx \frac{\sum_{j=0}^M u(z^{(j)}) \phi_i(z^{(j)}) w^{(j)}}{\sum_{j=0}^M \phi_i^2(z^{(j)}) w^{(j)}}, \quad (22)$$

where $\{(z^{(j)}, w^{(j)})\}_{j=0}^M$ are Gauss-type quadrature points that can be readily obtained using the Golub-Welsch method [18]. These rules are exact when the integrand have a polynomial order up to $2M + 1$. The method is thus fully non-intrusive, since only deterministic solutions at particular points of the stochastic space are needed. This procedure differs from the classical Monte Carlo method only by the sampling technique used to select collocation nodes in the associated stochastic space.

Let now $\mathbf{Z} : \Omega \rightarrow \mathbb{R}^d$ be a vector of independent random variables Z_1, \dots, Z_d with densities $\rho_{z_1}, \dots, \rho_{z_d}$. It holds that $\rho_{\mathbf{z}}(\mathbf{z}) = \prod_{i=1}^d \rho_{z_i}(z_i)$, due to the independence condition. A possible set of basis functions for $L^2_{\rho_{\mathbf{z}}}$ is given by $\{\Phi_{\mathbf{i}}\}_{\max_{\mathbf{i}} i \leq P}$ where $\mathbf{i} = (i_1, \dots, i_d)$ is a multi-index and

$$\Phi_{\mathbf{i}}(\mathbf{z}) = \phi_{i_1}(z_1) \cdot \dots \cdot \phi_{i_d}(z_d). \quad (23)$$

This construction includes P^d basis functions and is more accurate than the required order P . An alternative set of basis is given by $\{\Phi_{\mathbf{i}}\}_{|\mathbf{i}|=0}^P$, where $|\mathbf{i}| = \sum_{j=1}^d i_j$. For this set of basis

$$\dim \left(\text{span} \{ \Phi_{\mathbf{i}} \}_{|\mathbf{i}|=0}^P \right) = \binom{N+d}{N}, \quad (24)$$

that is more tractable than P^d . The computation of the coefficients in the multidimensional gPC-expansion is again possible using Gauss-type quadrature rules. Both of these constructions are based on the tensor product of 1-dimensional rules and thus are computationally expensive: for a 1-dimensional quadrature rule using M points, the d -dimensional cubature rule uses M^d points. This effect is called *curse of dimensionality*.

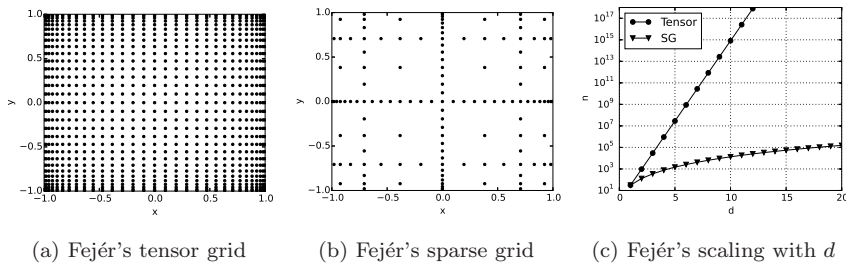


Fig. 2: A tensor grid and a sparse grid of order $l = 5$ based on Fejér's quadrature rule [14,33]. On the right it is illustrated how the number of quadrature points scale with respect to d for $l = 5$.

Before addressing the curse of dimensionality, we need first to observe that quadrature rules based on the zeros of orthogonal polynomials are not *nested* in general, meaning that the quadrature points Θ_l based on the polynomial of order l are not in $\Theta_{l'}$, with $l' \geq l$. This property is important in practical calculations in case we would like to increase the accuracy but we don't want to waste results already computed. Common choices of nested quadrature rules are the Clenshaw-Curtis and Fejér's [8,14,33], that uses the maxima of the Chebyshev polynomials as quadrature points, and the Kronrod-Patterson rules [20]. With appropriate scaling, this quadrature rule works on the bounded interval $[0, 1]$ with a probability density function $\rho(z) = 1$, corresponding to the uniform distribution. In general we will have to compute integrals as in (22), where ρ_z does not need to be the uniform density function. However, using the fact that the CDF F_z is bijective, we can use a variable transformation s.t.

$$\int_{\mathbb{R}} f(z)\rho_z(z)dz = \int_0^1 g(x)dx, \quad g(x) \equiv f(F_z^{-1}(x)). \quad (25)$$

Using these nested rules, we can attempt to alleviate the curse of dimensionality. One particularly successful approach is given by *Sparse Grids* (see [28,9] for details). The idea is not to take the complete tensor product of the 1-dimensional grids, but only products up to the desired order for each stochastic dimension, very much alike the construction of the set of basis $\{\Phi_{\mathbf{i}}\}_{|\mathbf{i}|=0}^P$. This procedure assumes a certain level of separability of the function, meaning that the cross-contribution of the parameters is lower than the contribution of the parameters considered separately. Figure 2 shows a comparison of tensor grids and sparse grids. From figure 2c we can see that the gain given by sparse grids over tensor grids increases with the stochastic dimension d . Using sparse grids the curse of dimensionality is alleviated, even if good accuracy in high dimensions is still a demanding task.

4 Uncertainty Quantification in Nonlinear Water Wave Simulations

We now use the stochastic formulation given in (8) to describe the stochastic evolution of water waves. We seek the stochastic free surface position $\zeta(\mathbf{x}, t, \mathbf{Z})$ and the stochastic velocity potential $\tilde{\phi}(\mathbf{x}, t, \mathbf{Z})$. For both the Monte Carlo approach and the Stochastic Collocation method, we need to solve (8) at a set of points $\{\mathbf{z}^{(i)}\}_{i=1}^N$, producing the ensemble of solutions

$$\left\{ \zeta(\mathbf{x}, t, \mathbf{z}^{(i)}) \right\}_{i=1}^N, \text{ and } \left\{ \tilde{\phi}(\mathbf{x}, t, \mathbf{z}^{(i)}) \right\}_{i=1}^N. \quad (26)$$

The sampling strategy depends on the particular method chosen. Furthermore, the Stochastic Collocation Method constructs surrogate functions

$$\zeta(\mathbf{x}, t, \mathbf{Z}) \approx P_N \zeta(\mathbf{x}, t, \mathbf{Z}) = \sum_{|\mathbf{i}| \leq N} \hat{\zeta}_{\mathbf{i}}(\mathbf{x}, t) \Phi_{\mathbf{i}}(\mathbf{Z}), \quad (27a)$$

$$\tilde{\phi}(\mathbf{x}, t, \mathbf{Z}) \approx P_N \tilde{\phi}(\mathbf{x}, t, \mathbf{Z}) = \sum_{|\mathbf{i}| \leq N} \hat{\phi}_{\mathbf{i}}(\mathbf{x}, t) \Phi_{\mathbf{i}}(\mathbf{Z}), \quad (27b)$$

that provide an easy way to compute statistics and to reproduce the PDFs of the solution variables.

In the following, we revisit two classical benchmarks to illustrate how uncertainty quantification can be done efficiently. Even if both Monte Carlo method and Stochastic Collocation method have been employed, due to space constraint, only the figures obtained using SCM will be shown. In all the cases presented the results agree for the two methods and SCM shows faster convergence and thus requires much fewer realizations, resulting in reduced CPU time.

4.1 Harmonic generation over a submerged bar

We now consider an experimental setting originally proposed by Beji and Battjes (1994) [1]. In the experiment a nonlinear wave propagates across a submerged bar. In the process the bound wave harmonics are decomposed into free harmonics which are released on the lee side of the bar and causes a transformation of the initial wave profile as described in [2]. It is generally accepted that the experiment can be reproduced within engineering accuracy by a verified deterministic wave model such as (1), which describe both the nonlinear and dispersive effects accurately. However, calibration details and measurement errors are not included in the public report by Beji and Battjes. Therefore, in the following, we will assume uncertainties and detail how these can be accounted for in the stochastic simulations.

To analyze the wave evolution we use the bottom topography of the experiments shown in figure 1. We consider the setup corresponding to Case A in the original experiments [2], where the input wave signal is defined by a wave

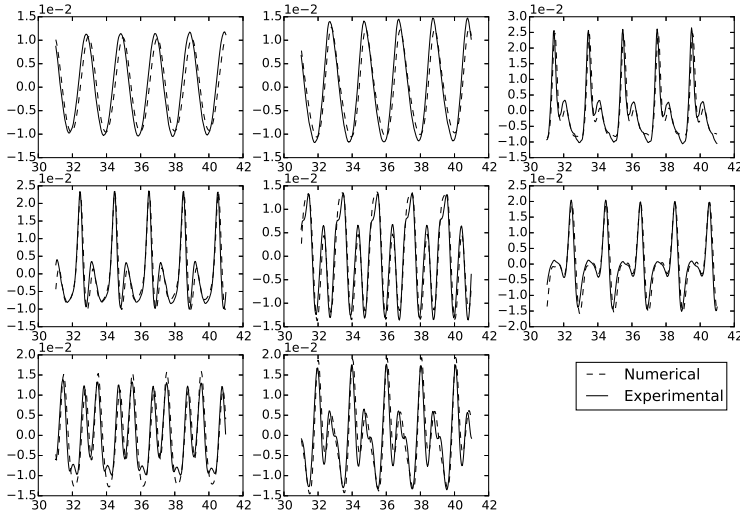


Fig. 3: Deterministic solution of the submerged bar experiment at eight different gauge locations. The experimental data are due to Luth *et al.* [23].

period $T = 2.02\text{s}$ and a wave height $H = 2\text{cm}$. In the numerical solver the input waves are generated using Stokes second order theory.

The shape of the bar and the shape of the incoming wave influence the spectrum of the waves that reach the right end of the domain as analyzed in [2]. In the following different sources of uncertainties are considered and the results are compared with deterministic results often presented in existing literature as well as to the experimental measurements due to Luth *et al.* [23].

4.1.1 Deterministic results

As a conventional mean for validation of the numerical wave model, we compare with the experimental measurements at eight gauges positioned in the wave tank. The results of this comparison are presented in Figure 3, where the bathymetry used is the exact bathymetry illustrated in figure 1. The results have been computed with the parameters of the experiment given in table 1. These parameters will be changed in the following to reflect single realizations of uncertain parameters. Clearly, the computation and the experiments match qualitatively very well, however there are noticeable discrepancies between the numerical calculations and the experimental data. For example, the wave heights and phases are not exactly reproduced at the first and second measurement stations. Discrepancies in the wave signal are observed at the high peaks in measurements from stations 5, 7 and 9, and in the low and intermediate peaks of station 6. The numerical calculations are done using

Description	Variable	Value
Bar height from bottom	h_{bar}	$0.3m$
Bottom floor	h_b	$-0.4m$
Entering wave length	T	$2.02m$
Basin Length		$29.0m$
Gauges positions		$\{4.0, 10.5, 13.5, 14.5, 15.7, 17.3, 19.0, 21.0\}$

Table 1: Nominal values and experimental settings used for the deterministic solution of the water wave problem.

a high-order accurate numerical method [11] with sufficient resolution to accurately resolve the dispersion and nonlinear wave effects, and are therefore assumed to be converged to a grid-independent solution. The absorption zone introduced behind the bar has been defined so that minimum wave reflections occur. However, discrepancies between experiments that are due to uncertainties in the measurement data or experimental setup are not taken into account in the numerical results. This motivates the studies in the following, where we will investigate the effects of taking into account the uncertainty in the model input.

4.1.2 Uncertain still water height

A very difficult parameter to be controlled when experiments in a manufactured basin are performed, is the exact height of the still water. In particular the accuracy of the measured height is sensitive to fluctuations, evaporation and spill of water. Here we use the truncated normal distribution

$$h_b \sim \text{trN}(0.3m, 0.0125^2m^2, [0.375m, 0.425m]) \quad (28)$$

to represent the fact that large defects in the water height can be detected and corrected.

Figure 4 shows the mean and standard deviation of the solution computed with SCM with 11 realizations. We can notice that the mean value seem not to follow the experimental solution on top and downstream of the bar. To shed more light on the characteristics of the distribution of the solution, we need to look at its PDF. We can use the surrogate model (19) of the solution, obtained by the SCM, to evaluate a high number of approximate realizations of the model with insignificant computational burden. We generate in this way 10^4 realizations sampled from the distribution (28). The surrogate solutions are then organized in histograms and which are shown in figure 5. In spite of being generated by a Gaussian input uncertainty, the distribution of the solution is not Gaussian and higher statistical moments have developed during the propagation of such uncertainties. In particular we can see that at certain times, the distribution is even bimodal due to an uncertain phase shift.

The quality of the surrogate model (19) can be checked inspecting the decay of the expansion coefficients (19). If the solutions change smoothly in the parameter space (h_b), then the convergence is expected to be very fast,

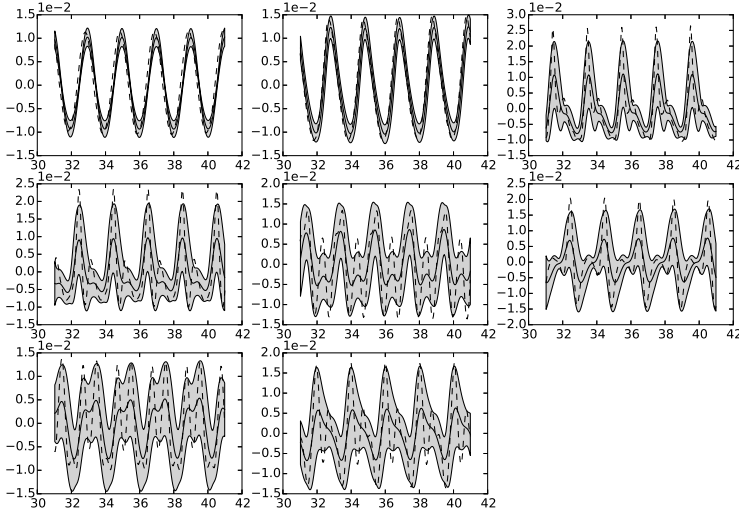


Fig. 4: Mean (solid line) and standard deviation (shaded) of the solution of the submerged bar experiment with $h_b \sim \text{tr}\mathcal{N}(0.3m, 0.0125^2m^2, [0.275m, 0.325m])$ at the different measurement locations, obtained by the SCM with 11 realizations. The experimental data (dashed) is also shown.

in the best case *spectral* [5]. Figure 6 shows the time varying values of the coefficients in the \log_{10} scale. We can notice a clear periodicity in the values of the coefficients. This highlights that the expansion order needed to reach a required accuracy may vary over time and care should be taken to select an appropriate expansion order for the analysis to be accurate.

The convergence rates of the MC and the SCM methods are shown in Fig. 7a. Here, for each gauge, the L^2 error in the estimated time-varying mean is computed against an highly accurate reference solution obtained using SCM with polynomial order 20. The convergence is shown in terms of number of function evaluations. Assuming that the computational complexity of the deterministic problem is mildly dependent on the examined parameters, the number of function evaluations is linear to the CPU time required. We can recognize the convergences on the first two gauges which are significantly faster. The MC method shows its characteristic slow convergence, while the SCM exhibit *spectral* convergence.

4.1.3 Uncertain input wave length

A parameter which is difficult to reproduce accurately in practical experiments is the input wave signal. An accurate representation of the wave signal requires that the wave maker displacement and the wave amplitudes are matched. This

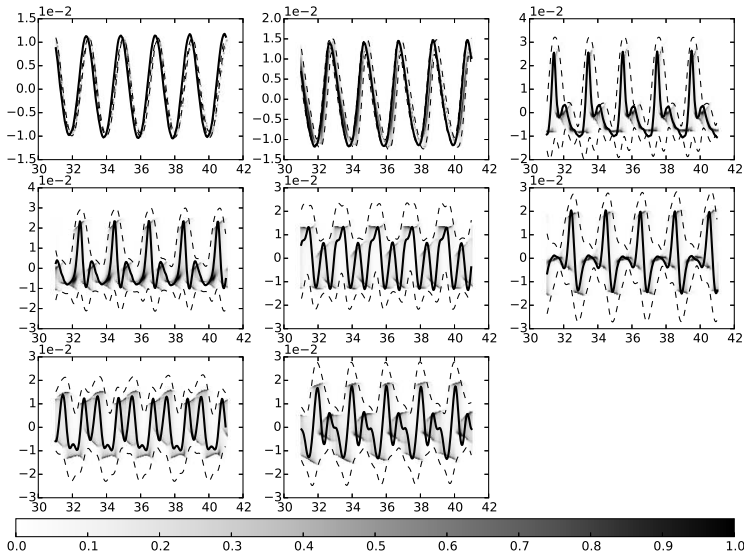


Fig. 5: Probability distributions of the time-varying solution of the submerged bar experiment with $h_b \sim \text{tr}\mathcal{N}(0.3, 0.0125^2, [0.275, 0.325])$ m at different measurement locations. These results are obtained by the SCM with 11 realizations. The thick black lines show the experimental results at the different gauges, while the dashed lines show the 95% confidence intervals.

can be difficult to achieve in practice, especially for nonlinear wave signals, and may lead to harmonic generation. To illustrate how such uncertainty in the signal can be accounted for, we use

$$T \sim \mathcal{N}(2.02s, 0.01^2s^2) \quad (29)$$

to represent the uncertainty due to the generation of the input waves.

Using the surrogate model provided by (19), we can reproduce the time dependent probability distribution of the solution shown in figure 8. We can observe that the uncertainty on the input wave length gives a relatively small contribution to the uncertainty of the solution. A comparison of the convergence of the MC method and the SCM method is shown in Fig. 7b.

4.1.4 Two dimensional uncertainty on wave length and water height

In many practical cases uncertainty does not enter a dynamical system only through one coefficient, but as a combination of multiple uncertainties. The still water height and the input wave length enter the system independently, however they will have a combined influence on the uncertainty of the solution. We will use the distributions (28) and (29) as in the previous examples. We

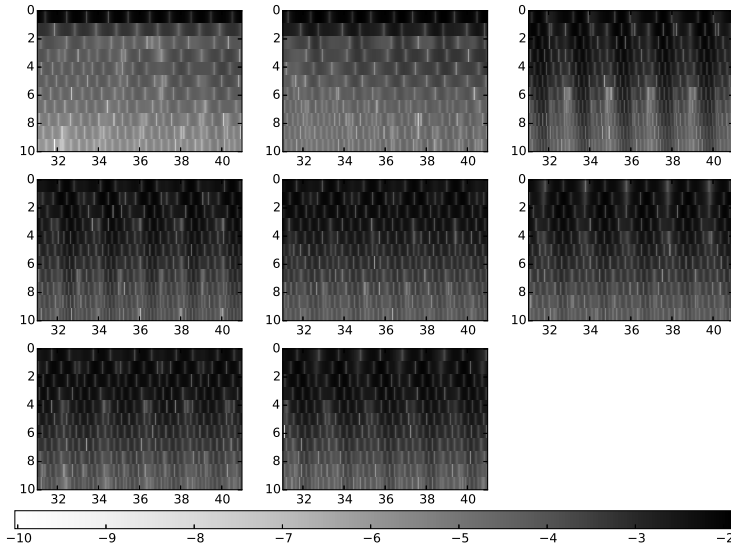


Fig. 6: Decay of the gPC-expansion coefficients in (19). The time varying coefficients values are shown in the \log_{10} scale according to the colors in the color bar.

expect the variance of the solution to increase due to the higher quantity of uncertainty allowed in the system. Figure 9 shows the time dependent distribution function of the solution. We can observe that the obtained uncertainty is not merely the superposition of the uncertainties obtained in the one dimensional cases (see fig. 5 and fig. 8), but is increased due to the interaction between the two. This effect will be more evident through the observation of the coefficients in the gPC expansion (19).

High order cubature rules of order 20 were used in the gPC method. This expansion order was found sufficient to get enough accuracy in the construction of the surrogate function (19). Figure 10 shows the decay of the projection coefficients in relation to both the input uncertainties. A total independence of the two parameters in the influence of the system would produce an expansion (19) where all the non-zero coefficients $\hat{f}_{\mathbf{i}}$ are the ones with $\mathbf{i} = (i, 0)$ or $\mathbf{i} = (0, j)$, $i, j = 0, \dots, 20$. This corresponds to have decays similar to the one shown in the first upper-left plot in figure 10. The next plots, however, show that the two input uncertainties act on the solution in non-trivial ways when combined. This means that the results of the UQ analysis on the two separate sources, cannot be trivially superposed, but they need to be considered together in a unique UQ analysis. Furthermore, the application of Sparse Grids on this case would suffer from this property which corresponds to the lack of separability

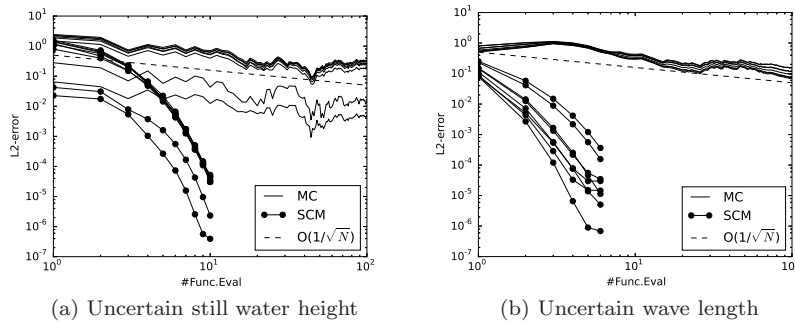


Fig. 7: Convergence rate of the MC method and the SCM method. The L^2 error of the approximation of 10s of simulation is computed against an highly accurate reference solution of order 20. The different lines belong to different gauges. The MC method exhibit its slow convergence of $\mathcal{O}(1/\sqrt{N})$. The SCM method shows *spectral* convergence.

of the function of interest. Methods which allow a sparse sampling in these situations are still lacking in the scientific literature.

4.1.5 Uncertain bottom topography

The topography of the basin is often precise in experimental settings, but rarely for real sites. Small discrepancies with respect to the ideal design can still be present. We will model these discrepancies using a Gaussian random field added on top of the deterministic basin, as shown in figure 1. In particular we will consider a Gaussian random field with exponential covariance (11) and with correlation length $a = 1.0$. The mean of the field is set to be the nominal bottom topography and the total variance of the field is set to $\sigma^2 = 0.01^2$. One realization of such random field is shown in figure 1a. With this model we try to capture small macroscopic errors in the slope of the basin's bottom. The random field is expanded using the KL-expansion (9), capturing 95% of the total variance of the field. This results in a truncated KL-expansion with 3 terms.

The Sparse Grid method introduced in Section 3.2.1 is used here with order $l = 3$ to compute mean and variance of the free surface profile at the eight measuring stations. Figure 11 shows the results obtained using only 19 realizations of the deterministic model. We can see that the uncertain bottom topography considered plays an important role in the wave transformation downstream of the bar, even if the random field considered has a relatively long correlation length and small variance.

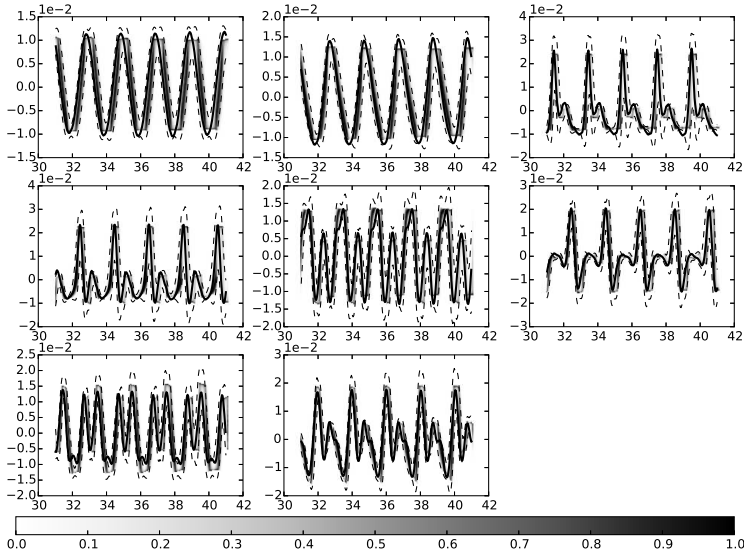


Fig. 8: Probability distributions of the time-varying solution of the submerged bar experiment with input wave length $T \sim \mathcal{N}(2.02s, 0.01^2s^2)$ at different measurement locations. The thick black lines show the experimental results at the different gauges, while the dashed lines show the 95% confidence intervals.

4.2 Harmonic generation over a semi-circular shoal

Extending the analysis to the full three dimensional problem we will proceed to the experiments of Whalin [34]. The experiments consists of a regular wave propagating over a semi-circular shoal, see figure 12a. The shoaling process transfer energy between the bound harmonics but, in contrast to the submerged bar case, the harmonics remain bounded and refraction adds complexity to the solution. The Whalin experiments have become standard benchmarks for dispersive wave models regardless of a rather substantial scatter present in the experimental data. We will look into the case of incoming waves with height $H = 0.015$ m and period $T = 2$ s. For this case most numerical models tend to over predict the amplitude of the second harmonic. As the present model is able to accurately capture all the major phenomena taking place in the experiments we are interested to see what level of uncertainty this corresponds to in the experimental values.

The deterministic numerical solution is computed for $t \in [0, 50]$ and then compared with the experimental measurements of the magnitude of the first three harmonics at different measurement locations through the center plane. Figure 12b shows the fitting of the numerical solution to the measurement data. The aim of the next sections is to study how the uncertainty in some

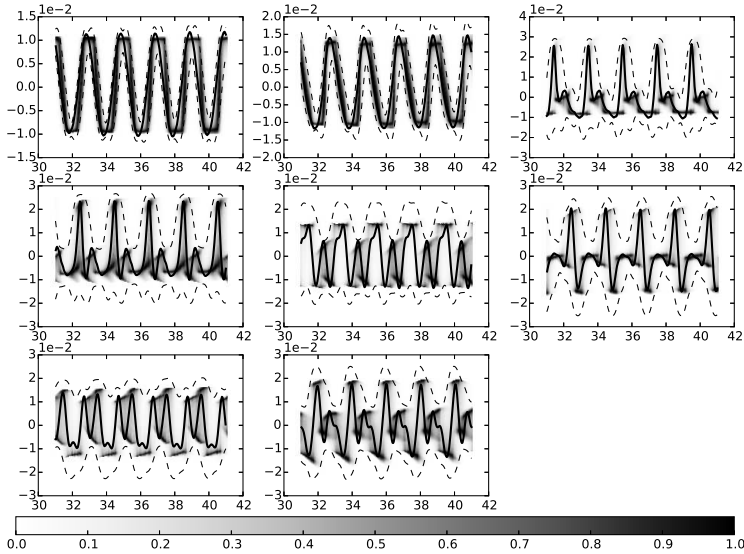


Fig. 9: Probability distributions of the time-varying solution of the submerged bar experiment with uncertain still water height h_b and wave length T , at different measurement locations. The thick black lines show the experimental results at the different gauges, while the dashed lines show the 95% confidence intervals.

experimental parameters can influence the results. Without presumption of causality, this analysis can highlight parameters that can influence results more deeply than others. The computational cost of solving the full three dimensional problem calls for efficient UQ methodologies that require the minimum number of simulations to make analysis practically feasible.

4.2.1 One dimensional uncertainties

Building up on the experience acquired on the two dimensional case and from experimental knowledge, we will focus our attention to the two parameters that are most difficult to match, namely the input wave period and height. Due to the lack of information about how accurate experiments can be, we will assume that the input parameters are described by a Gaussian distribution and we will try to evaluate how sensitive the system is to single uncertainties, and, in the next section, to the combination of the two. We will model the wave height and the wave period with Gaussian distributions centered on their nominal values and with 5% standard deviation.

A stochastic collocation approach with estimation of the generalized Polynomial Chaos expansion (19) is adopted, with the order dictated by the accuracy required. Figure 13 shows the mean and the 95% confidence interval as

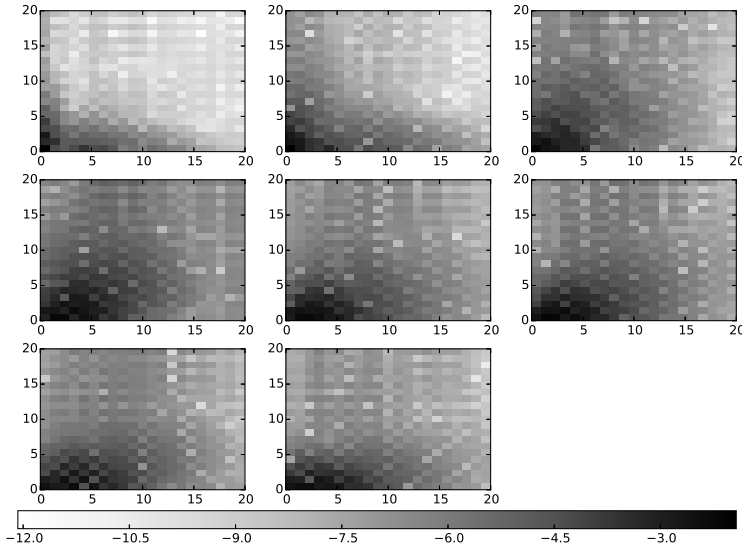


Fig. 10: Decay of the 2-dimensional gPC-expansion coefficients in (19) for the last integration time at different measurement locations. The coefficient values are shown in the \log_{10} scale according to the colors in the color bar.

well as the space-dependent distribution of the harmonics and the fitting with the experimental data.

4.3 Two dimensional uncertainty

The same problem setting is now investigated with uncertainty on the wave height and period at the same time. The same distributions used in the one dimensional setting are used here for the uncertainty sources. The Stochastic Collocation Method of order 5 is used to compute the space dependent probability distribution of the first three harmonics of the propagated wave. A total of only 36 deterministic simulations are required to obtain the desired approximation.

Figures 14 shows the space dependent mean and 95% confidence interval of the first three harmonics, as well as their space dependent probability distribution. Again we can notice that the resulting uncertainty – measured in variance of the solution – is not the mere superposition of the variances obtained with one dimensional uncertainties (see fig. 13). The probability distribution of the first three harmonics seem now to include the experimental measurements within some high probability region.

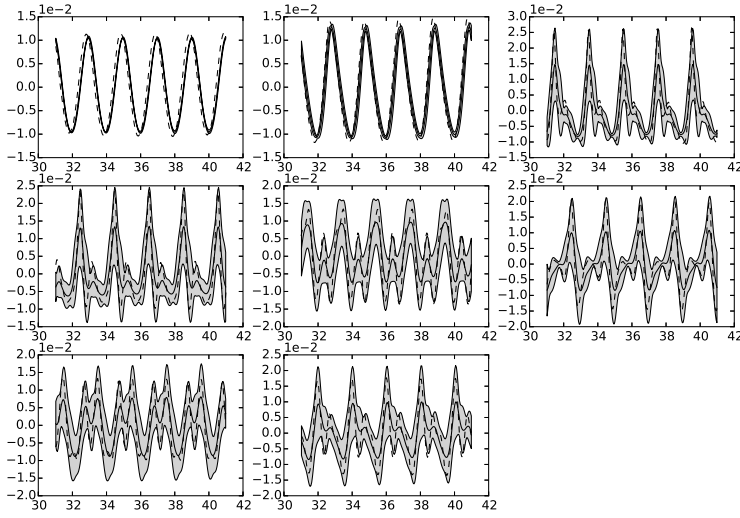
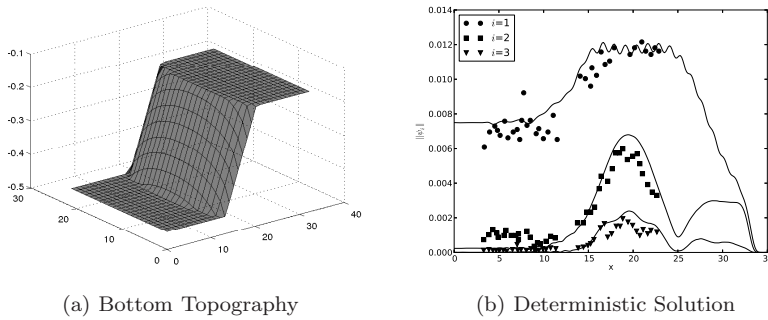


Fig. 11: Mean (solid line) and standard deviation (shaded) of the solution of the submerged bar experiment with the bottom topography described by a Gaussian random field with Ornstein-Uhlenbeck [31] covariance function at the different measurement locations. The experimental data (dashed line) is also shown. The results are obtained using the Sparse Grid method with 19 function evaluations.



(a) Bottom Topography

(b) Deterministic Solution

Fig. 12: Deterministic solution of the wave propagation in three dimensions. The first three harmonics of the numerical solution (full lines) for the center-line are compared with the corresponding experimental measurements at different longitudinal locations in the basin (dots).

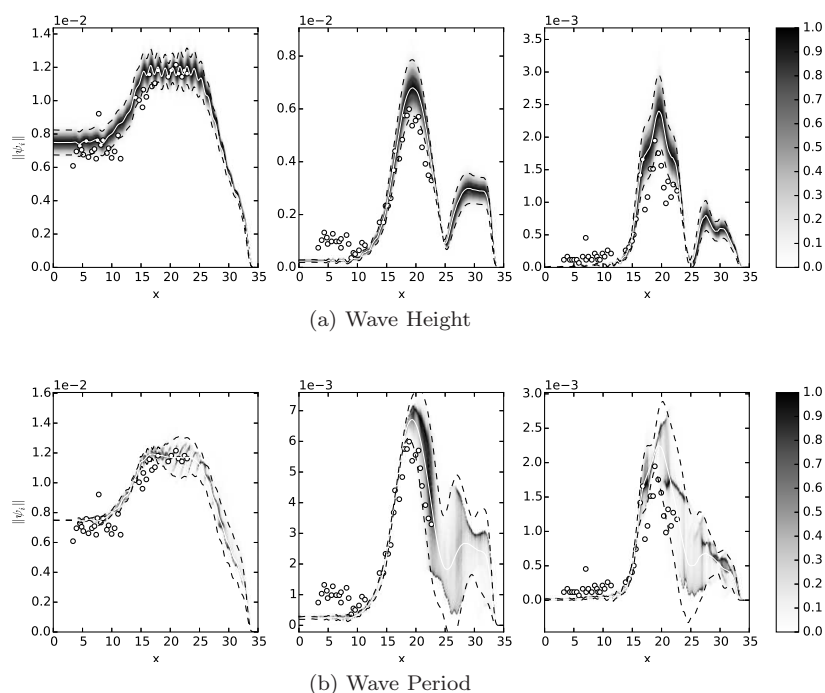


Fig. 13: Reconstructed space-dependent probability distribution function of the three harmonics of the solution of the Whalin test with one dimensional uncertainty. The white line shows the space-dependent mean, while the dashed lines show the 95% confidence interval around the mean. The scattered dots show the experimental data results.

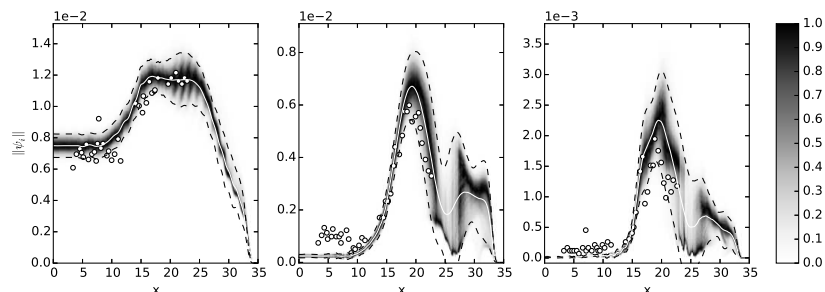


Fig. 14: Space-dependent probability distribution function of the Whalin test with two-dimensional uncertainty. The white solid line represent the mean for the three harmonics. The dashed lines show the 95% confidence interval around the mean. The scattered dots are the experimental measurements.

5 Conclusions

The Stochastic Collocation method (SCM) for Uncertainty Quantification (UQ) has been applied to a variety of stochastic wave problems, where the stochastic parameter space is low-dimensional. Numerical experiments have been carried out adopting often used standard benchmarks for wave models to create new stochastic benchmarks. The type of uncertainties accounted are those that are likely to appear in experimental settings, such as the input wave characteristics, the water height, and the topography of manufactured basins. With the aim of constructing stochastic benchmarks, we made reasonable assumptions regarding the distribution of such uncertainties, that would otherwise need to be characterized by extensive measurements or by a better description of the believed distributions. The focus in this work is toward the approximation of the probability distributions of observable Quantities of Interest (QoIs) and the exploration of the available methods able to reach this goal with the lowest computational burden.

The UQ methods selected here are all designed to tackle types of problems where obtaining a single deterministic solution is computationally expensive. The SCM, in its tensor form or in a sparse grid form, allows for high accuracy, due to the possibility of spectral convergence of the approximation, using a small number of deterministic solutions of the problem, that are obtained in a non-intrusive way. This allows the adoption of existing solvers, whose source code might be complex or not even available. In this work we use a high-order finite difference method for a fully nonlinear and dispersive medium-scale water wave model [11]. Thanks to the advent of High Performance Computing [12], large-scale water wave simulations are becoming more and more efficient and are subject of ongoing research.

On the downside of the SCM there is the fact that it is only suitable for problems with a low-dimensional stochastic space. Reminding that each problem has its own peculiarities (e.g. stochastic dimension, deterministic computational complexity, etc.), we are aware that as the stochastic dimension increases, the number of required solutions of the deterministic model increases more than polynomially, getting quickly not feasible. At the current state of research, these cases must be addressed using pseudo-random sampling techniques, whose convergence is slow but independent from the stochastic dimensionality. It is however important to remind that the latter techniques aim at the approximation of the output distribution through the approximation of its moments and this gets increasingly expensive if the target distribution has many non-zero high moments.

It is also important to observe that not all high-dimensional problems are really high-dimensional. One case was shown for the uncertain bottom topography in the submerged bar experiment, where the random field describing the perturbation of the topography has some regularity properties and can be parametrized via the KL-expansion, transforming an ideally infinite dimensional problem to a finite dimensional one.

The analysis performed on the new stochastic benchmarks show that the uncertainties on the input wave characteristics and the bottom topography have indeed a relevant effect on the free surface solutions. These effects are amplified when these uncertainties are considered simultaneously, leading to a non trivial transformation of the input probability distribution. The results of such analysis can be considered when explaining some of the discrepancy between numerical solutions and experimental results. In ongoing works we are considering problems with higher stochastic dimensions, resorting to novel techniques for deterministic sampling, such as Adaptive Sparse Grids [9] and Spectral Tensor Train decomposition [3].

The frameworks for random sampling² and for SCM³, as well as the results obtained in this work⁴, are made available on-line and are general enough to be applied on both small-scale and large-scale problems with no additional implementation burden.

References

1. Beji, S., Battjes, J.A.: Numerical simulation of nonlinear-wave propagation over a bar. *Coastal Engineering* **23**, 1–16 (1994)
2. Benxia, L., Xiping, Y.: Wave decomposition phenomenon and spectrum evolution over submerged bars. *Acta Oceanologica Sinica* **28**(3), 82–92 (2009)
3. Bigoni, D., Engsig-Karup, A.P., Marzouk, Y.M.: Spectral tensor-train decomposition (2014)
4. Boyaval, S., LeBris, C., Lelièvre, T., Maday, Y., Nguyen, N.C., Patera, a.T.: Reduced Basis Techniques for Stochastic Problems. *Archives of Computational Methods in Engineering* **17**(4), 435–454 (2010)
5. Canuto, C., Hussaini, M., Quarteroni, A., Zang, T.: Spectral Methods - Fundamentals in Single Domains. Scientific Computation. Springer Berlin Heidelberg, Berlin, Heidelberg (2006)
6. Cheng, M., Hou, T.Y., Zhang, Z.: A dynamically bi-orthogonal method for time-dependent stochastic partial differential equations I: Derivation and algorithms. *Journal of Computational Physics* **242**, 843–868 (2013)
7. Cheng, M., Hou, T.Y., Zhang, Z.: A dynamically bi-orthogonal method for time-dependent stochastic partial differential equations II: Adaptivity and generalizations. *Journal of Computational Physics* **242**, 753–776 (2013)
8. Clenshaw, C.W., Curtis, A.R.: A method for numerical integration on an automatic computer. *Numerische Mathematik* **2**(1), 197–205 (1960)
9. Conrad, P., Marzouk, Y.: Adaptive Smolyak pseudospectral approximations. *SIAM Journal on Scientific Computing* **35**(6), 2643–2670 (2013)
10. Dutykh, D., Clamond, D.: Efficient computation of steady solitary gravity waves (2013)
11. Engsig-Karup, A.P., Bingham, H.B., Lindberg, O.: An efficient flexible-order model for 3d nonlinear water waves. *Journal of Computational Physics* **228**, 2100–2118 (2008)
12. Engsig-Karup, A.P., Glimberg, L.S., Nielsen, A.S., Lindberg, O.: Fast hydrodynamics on heterogenous many-core hardware. In: R. Couturier (ed.) *Designing Scientific Applications on GPUs, Lecture notes in computational science and engineering*. CRC Press / Taylor & Francis Group (2013)
13. Engsig-Karup, A.P., Madsen, M.G., Glimberg, S.L.: A massively parallel gpu-accelerated model for analysis of fully nonlinear free surface waves. *International Journal for Numerical Methods in Fluids* **70**(1), 20–36 (2011)

² <https://pypi.python.org/pypi/UQTtoolbox/>

³ <https://pypi.python.org/pypi/SpectralToolbox/>

⁴ <http://www2.compute.dtu.dk/~apek/OceanWave3D/>

14. Fejér, L.: Mechanische Quadraturen mit positiven Cotesschen Zahlen. *Math. Z.* **37**, 287–309 (1933)
15. Gautschi, W.: Algorithm 726: ORTHPOL;a package of routines for generating orthogonal polynomials and Gauss-type quadrature rules. *ACM Trans. Math. Softw.* **20**(1), 21–62 (1994)
16. Gautschi, W.: *Orthogonal Polynomials: Computation and Approximation*. Numerical Mathematics and Scientific Computation. Oxford University Press (2004)
17. Glimberg, L.S., Engsig-Karup, A.P., Dammann, B., Nielsen, A.S.: Development of high-performance software components for emerging architectures. In: R. Couturier (ed.) *Designing Scientific Applications on GPUs*, Lecture notes in computational science and engineering. CRC Press / Taylor & Francis Group (2013)
18. Golub, G.H., Welsch, J.H.: Calculation of Gauss Quadrature Rules. *Mathematics of Computation* **23**(106), 221–230 (1969)
19. Kiureghian, A., Ditlevsen, O.: Aleatory or epistemic? Does it matter? *Structural Safety* (2009)
20. Kronrod, A.S.: Nodes and Weights of Quadrature Formulas. English transl. from Russian, Consultants Bureau **35**(597) (1965)
21. Larsen, J., Dancy, H.: Open boundaries in short wave simulations - a new approach. *Coastal Engineering* **7**, 285–297 (1983)
22. Loève, M.: *Probability Theory*, vols. I-II, 4 edn. Comprehensive Manuals of Surgical Specialties. Springer, New York (1978)
23. Luth, H.R., Klopman, B., Kitou, N.: Projects 13G: Kinematics of waves breaking partially on an offshore bar: LDV measurements for waves with and without a net onshore current. *Technical report H1573*, Delft Hydraulics (1994)
24. Maitre, O.P.L., Knio, O.M.: *Spectral Methods for Uncertainty Quantification: With Applications to Computational Fluid Dynamics*. Springer (2010)
25. McKay, M., Beckman, R., Conover, W.: A Comparison of Three Methods for Selecting Values of Input Variables in the Analysis of Output From a Computer Code. *Technometrics* **41**(1), 55–61 (2000)
26. Morokoff, W.J., Caflisch, R.E.: Quasi-Monte Carlo Integration. *Journal of Computational Physics* **122**(2), 218–230 (1995)
27. Naess, A., Moan, T.: *Stochastic Dynamics of Marine Structures*. Cambridge University Press, Cambridge (2012)
28. Petras, K.: Smolyak cubature of given polynomial degree with few nodes for increasing dimension. *Numerische Mathematik* **93**(4), 729–753 (2003)
29. Sapsis, T.P., Lermusiaux, P.F.: Dynamically orthogonal field equations for continuous stochastic dynamical systems. *Physica D: Nonlinear Phenomena* **238**(23–24), 2347–2360 (2009)
30. Schwab, C., Todor, R.A.: KarhunenLoève approximation of random fields by generalized fast multipole methods. *Journal of Computational Physics* **217**(1), 100–122 (2006)
31. Uhlenbeck, G., Ornstein, L.: On the theory of the Brownian motion. *Physical review* **36**(1905) (1930)
32. Venturi, D.: On proper orthogonal decomposition of randomly perturbed fields with applications to flow past a cylinder and natural convection over a horizontal plate. *Journal of Fluid Mechanics* **559**, 215 (2006)
33. Waldvogel, J.: Fast Construction of the Fejér and ClenshawCurtis Quadrature Rules. *Bit Numerical Mathematics* **46**(1), 195–202 (2006)
34. Whalin, R.W.: The limit of applicability of linear wave refraction theory in convergence zone. Tech. Rep. H-71-3, US Army Corps of Engineers (1971)
35. Wojtkiewicz, S.J., Eldred, M., Field, R.J., Urbina, A., Red-Horse, J.: A toolkit for uncertainty quantification in large computational engineering models. In: *Proceedings of the 42nd AIAA/ASME/ASCE/AHS/ASC Structures, Structural Dynamics, and Materials Conference* (2001)
36. Xiu, D.: Fast numerical methods for stochastic computations: a review. *Communications in computational physics* **5**(2), 242–272 (2009)
37. Xiu, D.: *Numerical Methods for Stochastic Computations: A Spectral Method Approach*. Princeton University Press (2010)
38. Xiu, D., Karniadakis, G.E.: The wiener–askey polynomial chaos for stochastic differential equations. *SIAM J. Sci. Comput.* **24**(2), 619–644 (2002)